THE JOURNAL OF PHYSICAL CHEMISTRY B

Article

pubs.acs.org/JPCB

Rheophysical Properties of Fluorinated Nonionic Micellar Phases

R. Banchathanakij,[†] O. Greffier,[†] L. Bécu,[†] M. J. Stébé,[‡] J. L. Blin,[‡] and Jean P. Decruppe*,[†]

[†]Laboratoire de Physique des Milieux Denses, 1 Bd. D. F. Arago IPEC, CP87811, 57078 Metz Cedex 3, France

[‡] Equipe Physico-chimie des colloïdes, Faculté des sciences, SRSMC, UMR 7565 CNRS Nancy Université, BP 70239, 54506 Vandoeuvre les Nancy cedex, France

ABSTRACT: Micellar phases can be used as templates for the preparation of mesoporous silica materials. Fluorinated and hydrogenated surfactants can provide a large variety of well-defined micellar structures: spherical and cylindrical micelles as well as more complex structures such as lamellar or sponge phases can be formed in various thermodynamic conditions. However, the preparation of ordered mesoporous materials from these organized media is not always successful for a reason not known at the moment. It thus seems of the highest importance to properly characterize the micellar solution prior to the addition of the silica precursor during the material synthesis. In this paper, we describe some rheophysical properties of the micellar phase L_1 prepared with a fluorinated surfactant, the formula of which is $C_7F_{15}C_2H_4(OC_2H_4)_8OH$, labeled as $R_F^7(EO)_8$. This surfactant forms micelles in water, and the direct micellar phases have been characterized in a wide range of temperatures and surfactant concentrations. The rheological properties of the L_1 phase have also been studied as a function of temperature and concentration. Under steady and dynamic flow conditions, the solutions behave like Newtonian or shear thinning fluids depending on the temperature and surfactant concentration. A crossover between G' and G'' is observed in the solution at the concentration of 20 wt % and at the temperature of 10 °C, suggesting the presence of long entangled micelles in solution at this temperature. When subjected to the action of a shearing device, the 20 wt % solution becomes optically anisotropic and shows flow birefringence, but the average orientation of the micelles quantified by the extinction angle χ shows an unexpected behavior when the shear rate is gradually increased.

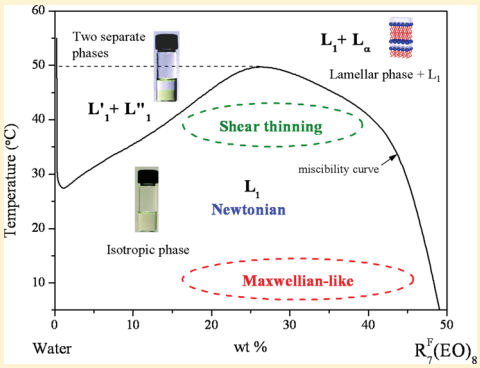

1. INTRODUCTION

Due to a wide range of applications and unique structural properties,[1,2] the synthesis of advanced mesoporous materials gives rise to an increasing interest and has been continuously developing in recent years. Their particular characteristics provide excellent opportunities for the creation of ordered materials with additional functionalities. For example, they can be used to trap enzymes such as lipases in order to design stable and reusable enzymatic bioreactors.[3]

The synthesis of mesoporous material is usually performed via a cheap and relatively simple sol−gel process.[4] The material is obtained from organized molecular systems which are used as a templating medium.[1−5] Interactions between a silica precursor and the aggregates formed by the surfactant molecules are at the origin of the formation of an hybrid organic−inorganic mesophase. The formation of this mesophase is initially based on a self-assembling mechanism between surfactant molecules and inorganic precursors; it is named the cooperative templating mechanism (CTM) or the cooperative self-assembling mechanism.[5−7] The preparation of mesoporous materials via the CTM mechanism requires a direct L_1 micellar phase in the initial step. However, it appears that the characteristics of the recovered materials, such as the structure and the pore diameter, are strongly related to the properties of the surfactant used for their preparation.[8−12]

The nonionic surfactant solutions usually have a miscibility curve (or lower consulate boundary, LCB) which separates a direct micellar domain (L_1) from a biphasic region in the [concentration, temperature] coordinate system.[13,14] The LCB is the locus of the cloud points (CPs), and the curve has a minimum corresponding to the critical point CP. Starting from a state in the L_1 phase and upon increasing the temperature, one crosses the LCB and the solution becomes turbid. The miscibility curve of the system fluorinated surfactant/water presents a critical point (CP) corresponding to a minimum value of the temperature. Although the value of hydrophilic−lipophilic balance lies in the range which corresponds to ordered hexagonal material (according to Stucky's rule),[15] the binary system studied in this work rather leads to the formation of a wormhole-like structure in the final product. The effect of adding different agents such as detergents, electrolytes, or certain organic fluids has been studied and reported to affect this cloud point.[16] However, the incorporation of fluorinated oil[17] and salt[18] into the micellar solution induces a shift of the miscibility curve toward higher temperatures, and after the CTM process, one gets mesoporous materials with an ordered hexagonal structure. Ordered mesoporous materials are not

Received: July 1, 2011
Revised: January 3, 2012
Published: January 9, 2012

ACS Publications © 2012 American Chemical Society

dx.doi.org/10.1021/jp2062139 | J. Phys. Chem. B 2012, 116, 1544−1550

always obtained from these organized surfactant structures. Thus, the self-assembly mechanism is favored if the lower consolute boundary is shifted toward high temperatures and if the phase separation temperature is moved away from the temperature at which the silica source is added to the micellar solution even if the template used is always a L_1 phase.

The aim of this work is to study the properties of the L_1 phase by nonequilibrium techniques and to bring information on the structure of the micelles in the solution.

We present here the results of rheophysical experiments (rheology and flow birefringence) performed on the $C_7F_{15}C_2H_4(OC_2H_4)_8OH$ ($R_7^F(EO)_8$)/water binary system at different temperatures and concentrations and subjected to steady and dynamic flows. The birefringence curves and especially the extinction angle variations with the shear rate show that the behavior of the L_1 micellar phase is different from that of a solution containing simple individual spherical micelles.

2. MATERIALS AND EXPERIMENTAL METHODS

2.1. Surfactant Solutions. The surfactant entering the preparation of the solutions is supplied by the company DuPont and is used without any further purification. It is a nonionic surfactant: the hydrophilic part consists of a series of oxyethylene groups ($-OC_2H_4-$), the average length of which is 8. The lipophilic tail consists of three different chain lengths, giving an average value corresponding to $C_7F_{15}C_2H_4-$. Although the raw material is a mixture of several chain lengths, in the following we shall use the formula $C_7F_{15}C_2H_4(OC_2H_4)_8OH$, abbreviated as $R_7^F(EO)_8$ to represent the molecule.

For the preparation of a series of samples at different concentrations, the necessary amounts of surfactant are carefully weighed (±0.01 g) and then dissolved in the required amount of water under magnetic stirring. The solutions are then stored at room temperature for several days in well-closed glass vials to avoid evaporation and to reach thermodynamic equilibrium prior to any measurement.

2.2. Phase Diagram. Although the phase diagram of the system $R_7^F(EO)_8$/water is already known,[10] we found it necessary to check it again since the samples were prepared with a different new batch of the surfactant.

The phase diagram of $R_7^F(EO)_8$/water is established by preparing a series of 16 samples in the concentrations range 0.5−50 wt % surfactant. Before each observation, the sample is left at rest for 20 min at least in a water bath at each controlled temperature. The different phases were merely identified by visual observation between crossed linear polarizers in natural white light. The liquid crystal phase domains are subsequently identified by direct observation of the texture under an optical microscope equipped with crossed polarizers. It is thus easy to identify the micellar and lamellar (L_α) phases and the phase separation in each vessel.

2.3. Rheology. Two rheometers were used to study the steady and dynamic properties of the various samples: a RFS III TA Instrument working in strain controlled mode and a stress controlled MCR 501 from Anton Paar. For both devices, measurements are conducted in a cone−plate cell (cone diameter = 50 mm, cone angle = 0.02 rad, and gap = 50 μm for RFSIII; cone diameter = 50 mm, cone angle = 1°, and gap = 103 μm for MRC 501); the temperature of the sample is kept constant within ±0.05 °C with a circulating bath or a Peltier regulator; a solvent trap is used to minimize the evaporation of the solvent. Three different kinds of experiments were performed: discrete shear rates ramps under steady state conditions, frequency sweep tests to follow the variations of the elastic moduli G' and G'', and, finally, stress cycles. During a steady state test, the sample is subjected to a series of increasing values of the shear rate $\dot{\gamma}$ (in strain controlled mode) or of the shear stress σ (in stress controlled experiments) for a finite time interval (usually 60−120 s); from these results, the viscosity curve $\eta(\dot{\gamma})$ is drawn and the rheological characteristics of the sample are deduced. From the second experiment, the distribution of G'' vs G' on a semicircle (Cole−Cole plot) reveals the Maxwellian character of the fluid. Finally, the micellar solution is subjected to a stress cycle which consists of a decreasing stress branch starting at a maximum value σ_M down to a minimum σ_m, followed by a constant stress at σ_m with recording of the viscosity as a function of time, and, finally, of a last branch during which the stress is again increased up to σ_M. This last stress sweep allows checking for the importance of the evaporation.

2.4. Flow Birefringence. Under the action of the shearing flow, the micellar solutions become anisotropic and flow birefringence experiments can then be conducted. Two quantities of interest can be deduced from the transmitted intensity signals: the extinction angle χ and the birefringence intensity $\Delta n = n_1 - n_2$; n_1 and n_2 are two of the three principal indexes of the anisotropic biaxial medium corresponding to vibrations in the plane perpendicular to the vorticity direction $\vec{\omega}$. The angle of extinction is particularly interesting since it brings information on the average orientation and size of the particles in the medium. Discrete shear rate ramps are the only birefringence experiments performed in a Couette device mounted on the polarimetric bench.

3. EXPERIMENTAL RESULTS AND DISCUSSION

3.1. Phase Diagram. The phase diagram of the binary system $R_7^F(EO)_8$/water is presented in Figure 1. The full lines

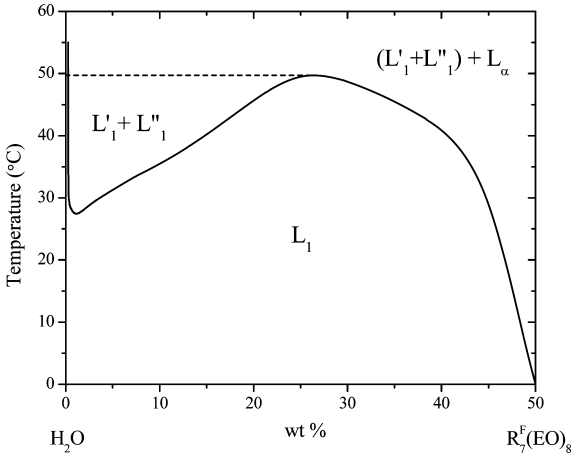

Figure 1. Binary phase diagram of $R_7^F(EO)_8$/water system. L_1, direct micellar phase; L_α, lamellar phase; $L'_1 + L''_1$, biphasic phase.

separate single phase domains from biphasic regions. The diagram has been established between 10 and 60 °C as a function of the surfactant concentration; a miscibility curve is found with a particular cloud point (critical point) at 27 °C for a concentration of 1 wt % in surfactant. Beyond the critical micellar concentration (cmc), self-organizing surfactant mole-

dx.doi.org/10.1021/jp2062139 | J. Phys. Chem. B 2012, 116, 1544−1550

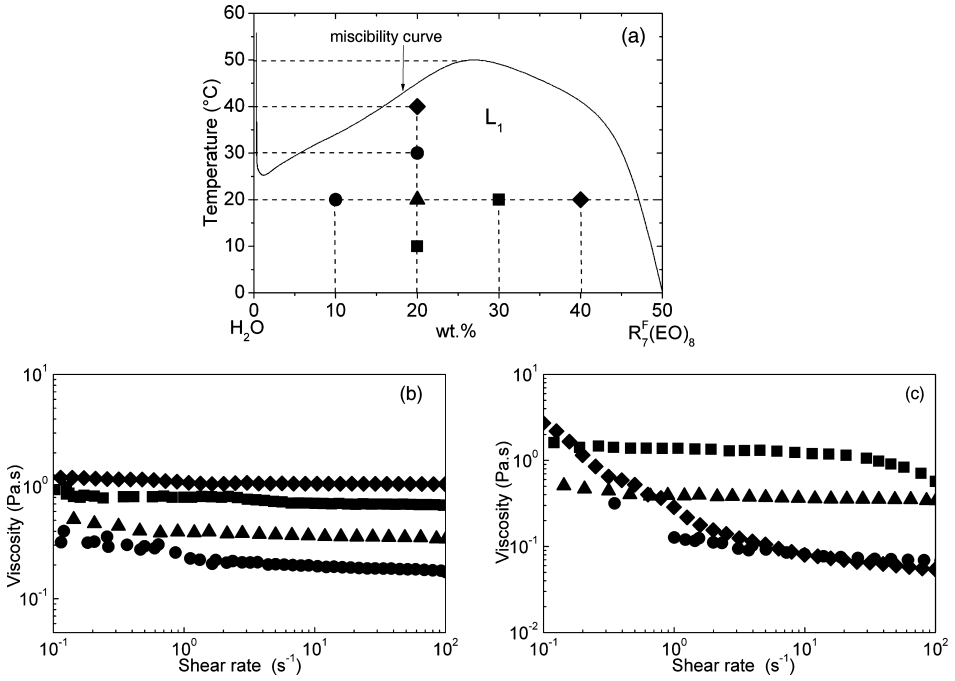

Figure 2. Rheological behavior in steady state shearing mode. (a) Miscibility curve (solid line) and, in the L_1 phase, symbols pointing out the solutions under investigation; (b) viscosity curves at 20 °C for various concentrations of (●) 10, (▲) 20, (■) 30, and (♦) 40 wt %; (c) viscosity curves at different temperatures for a concentration of 20 wt % and (■) 10, (▲) 20, (●) 30, and (♦) 40 °C.

cules can form aggregates of various sizes and shapes such as spherical or cylindrical micelles or lamellar and sponge phases. The miscibility curve in the lower concentration range ($[R_7^F(EO)_8]$ < 50 wt %) separates the isotropic L_1 phase from two biphasic domains. The two phases L'_1 and L''_1, respectively rich and poor in micelles, coexist in the low concentration range. In the middle range (between ~55 and 70 wt %), L_1 appears with a lamellar phase L_α. In the concentration range 70−90 wt %, a pure L_α phase is found (not represented in Figure 1). As the temperature is increased, the L_α concentration range is gradually narrowing and the phase disappears around 60 °C. At very high surfactant concentration, a reverse micellar phase (L_2) is formed.

3.2. Rheological Behavior. The quantitative analysis of the steady state measurements is done in the frame of the theoretical model with two parameters (Ostwald's law):

$$\sigma = \kappa\dot{\gamma}^n \quad (1)$$

or, if we introduce the apparent viscosity (η):

$$\eta = \kappa\dot{\gamma}^{n-1}$$

τ is the shear stress and $\dot{\gamma}$ is the shear rate; κ and n are both constants.

Experiments performed in dynamic mode lead to the elastic and loss moduli G' and G''. For a Maxwellian fluid, G' and G'' are

$$G' = G_0\frac{\omega^2{\tau_R}^2}{1+\omega^2{\tau_R}^2}$$

$$G'' = G_0\frac{\omega\tau_R}{1+\omega^2{\tau_R}^2}$$

τ_R is the relaxation time of the solution and ω is the angular frequency. Eliminating the product $\omega\tau_R$ in G' and G'' leads to the equation of a circle (Cole−Cole plot), and the Maxwellian character of the fluid can be appreciated by plotting G'' vs G'.

3.2.1. Steady State Rheological Behavior. The two parameters of this study are the surfactant concentration $[R_7^F(EO)_8]$ and the temperature T. The points representing the different solutions used for this study appear in the partial phase diagram (Figure 2a). They all are situated in the L_1 micellar phase domain.

Figure 2b describes the variations of the apparent viscosity η as a function of the shear rate on a log−log scale. Four solutions of concentrations 10, 20, 30, and 40 wt % are subjected to increasing shear rates in the range 0.1−10^2 s^{-1}, and the temperature is kept constant within the interval 20.00 ± 0.05 °C.

A qualitative observation of the distribution $\eta(\dot{\gamma})$ in Figure 2b shows at first an increase of the apparent viscosity with the concentration. Two types of rheological behavior can be distinguished. For the more concentrated solutions (30 and 40 wt %), the quasi-Newtonian behavior is found over the whole shear rate range. Fitting the experimental results with Ostwald's law (eq 1) leads to n = 0.99 and κ = 1.07 for a concentration of 40 wt % and n = 0.97 and κ = 0.76 for the 30 wt % sample. The value of n close to 1 confirms the highly Newtonian character of these two solutions. In the case of the two lowest concentrations (10 and 20 wt %), the variation of apparent viscosity η as a function of shear rate is discontinuous. As a matter of fact, the viscosity curve appears as formed by the juxtaposition of two approximately linear segments with different slopes in the log−log system; therefore, a simple model with two parameters cannot explain on its own the rheological behavior over the entire shear rate range. The change of the slope appears at a critical shear rate $\dot{\gamma}_c$ all the smaller as the surfactant concentrations is larger: $\dot{\gamma}_c \approx 0.7$ s^{-1} for $[R_7^F(EO)_8]$ = 20 wt % and $\dot{\gamma}_c \approx 2$ s^{-1} for $[R_7^F(EO)_8]$ = 10 wt %. In the low shear rate range, $\dot{\gamma} \in 0.1-\dot{\gamma}_c$ s^{-1}, the viscosity

dx.doi.org/10.1021/jp2062139 | J. Phys. Chem. B 2012, 116, 1544−1550

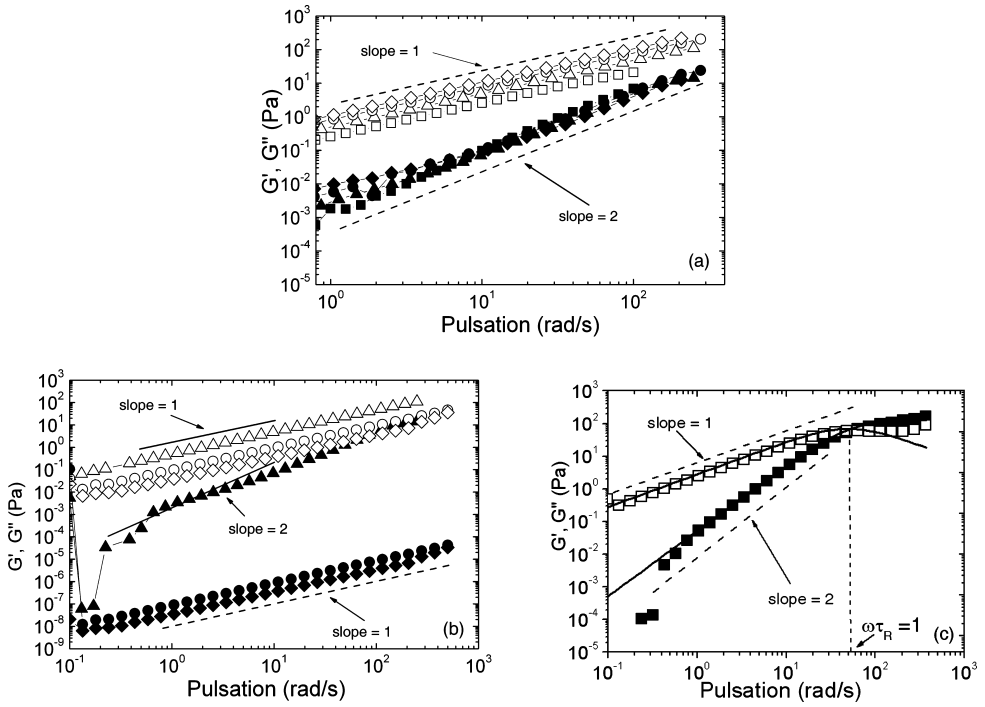

Figure 3. Storage modulus G' (solid symbols) and loss modulus G'' (open symbols) as a function of the angular frequency ω: (a) at a constant temperature of 20 °C and different concentrations of (■, □) 10, (▲, Δ) 20, (●, ○) 30, and (◇, ♦) 40 wt %; (b) at a constant concentration of 20 wt % and different temperatures of (▲, Δ) 20, (●, ○) 30, and (◇, ♦) 40 °C. (c) At a constant concentration of 20 wt % and 10 °C, G' (■) and G'' (□) intersect at the "crossover" point for which $\omega\tau_R = 1$. From the intersection coordinates, the computed relaxation time (τ_R) turns out to be 0.02 s. The solid curves represent Maxwell's theoretical model. Two dashed lines of slopes 1 and 2 are added to serve as a visual guide.

decreases and the shear thinning character is more important for the 10 wt % solution. This behavior may result from an orientation effect of the micelles under the action of the hydrodynamic field. In the highest gradient domain, the values of the two constants n and κ are computed by fitting the experimental data to the two-parameter model: one gets n = 0.97 and κ = 0.40 for the 20 wt % solution and n = 0.98 and κ = 0.20 for the 10 wt % sample. Again the constant n is close to 1 in good agreement with the Newtonian character observed at the highest shear rate (see Figure 2b).

The variations of apparent viscosity of the 20 wt % solution versus the shear rate at different temperatures, 10, 20, 30, and 40 °C, are reported in Figure 2c. Upon increasing the temperature, the solution (see Figure 2a) moves closer and closer to the miscibility curve and the temperature increase leads to a significant qualitative change in the viscosity curves.

At 10 °C, a quasi-Newtonian behavior is observed over a wide range of shear rates: the apparent viscosity η, almost constant in the range of low shear rate decreases, afterward, at higher shear rates. Then, as the temperature is increased, the initial Newtonian character disappears, the solution is shear thinning at low shear rates, and this character is even stronger for the highest temperature. This change in the rheological behavior related to the temperature rise is an indication of a structural change of the particles in solution. At 40 °C and low shear rates, the apparent viscosity η is greater than at 10 and 20 °C. Shrestha et al.[19] reported that an increase of the temperature results in an increase of the size of nonionic surfactant micelles and that one can expect the formation of long cylindrical micelles at higher temperatures. This hypothesis is consistent with the solution behavior at 40 °C; as a matter of fact, the fast decrease of the viscosity η under weak shearing reflects an easy orientation of the particles and the average orientation is all the faster as the micellar length is larger.

3.2.2. Dynamic Rheological Behavior. For this type of experiment, the solutions are subjected to a sinusoidal deformation in the linear strain region (strain = 2%). The maximum angular frequency is 500 rad/s.

The effect of the surfactant concentration at 20 °C is summarized in Figure 3a. At the given temperature of 20 °C, the overall behavior of the four solutions is the same: the storage modulus G' is always smaller than the loss modulus G''; the viscous character prevails over the entire frequency range. Apart from some fluctuations of the storage modulus G' at low frequencies probably due to the limitations of the equipment, the experimental distribution is close to the line of slope 2 (see Figure 3a, the dashed straight line); it is a corroboration of the viscoelastic characteristic of the solution. The loss modulus G'' distribution gather remarkably well around the line of slope 1.

The surfactant concentration being chosen at 20 wt %, we now consider the influence of the temperature increase on the behavior of G' and G''. The experimental distributions of G' and G'' as a function of the angular frequency (ω) are reported in Figure 3b,c. For the two highest temperatures (30 and 40 °C), the viscous character of the solution always predominates; the elastic modulus G', always very small, ranges $10^{-8} < G' < 10^{-6}$ Pa. For the two lowest temperatures (10 and 20 °C) and particularly for 10 °C (see Figure 3c), the variations of G' and G'' under sinusoidal strain are reminiscent of a Maxwellian fluid: $G'(\omega)$ is an increasing function of ω within the interval $5 \times 10^{-1} < \omega < 4 \times 10^{1}$ rad/s and $G'(\omega) \sim \omega^n$ with $n \sim 2$. In addition, at 10 °C, G' and G'' intersect at the "crossover" point for which $\omega\tau_R = 1$; $\tau_R = [\tau_{break}\tau_{rep}]^{1/2}$ is the terminal relaxation time, while τ_{break} is the breaking time of the micelles and τ_{rep} is

dx.doi.org/10.1021/jp2062139 | J. Phys. Chem. B 2012, 116, 1544–1550

the reptation time. From the "crossover" point,[20] we easily calculate the relaxation time $\tau_R \approx 0.02$ s.

In the range of high angular frequency ($\omega > 10^2$ rad/s), G' converges to the plateau modulus G_0, which is related to the zero shear viscosity and the relaxation time by

$$\eta_0 = G_0\tau_R$$

By averaging G' over the last few values obtained at high frequency, we obtain $G_0 \sim G'_{average} = 117$ Pa. Taking into account the calculated value of the relaxation time, we obtain for η_0 a value of 2.34 Pa·s, close to the value extrapolated from the viscosity curve at low shear rates (see Figure 2c, symbol ■).

The Maxwellian character of the solution clearly appears in Figure 4, where we have plotted the variations of G'' as a function of G' (Cole–Cole plot). The result of a fitting with Maxwell's theoretical model using 117 Pa for G_0 is represented by the continuous line. In the low frequency range, the theoretical curve is in good agreement with the experimental values; however, at high frequencies, G'' departs significantly from the circle, decreasing to a minimum G''_{min} before increasing again. The minimum G''_{min} occurs for the angular frequency $\omega = \omega^* = 207$ rad/s, from which we can compute the breaking time τ_{break} of the micelles:[20]

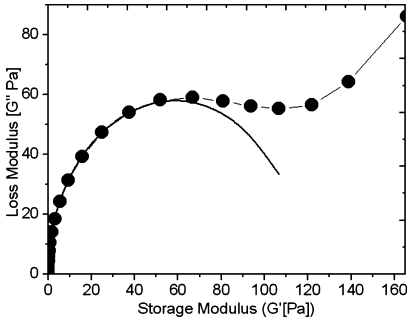

Figure 4. Cole–Cole plot G'' (G') of 20 wt % $R_7^F(EO)_8$ at 10 °C. Symbols (●) correspond to the experimental points, and the continuous curve represents the result of a fitting with a plateau modulus $G_0 = 117$ Pa.

$$\tau_{break} \approx \frac{1}{\omega^*} = 5 \text{ ms}$$

Also, from the plateau modulus G_0, one can compute the hydrodynamic correlation length ξ_H which can be regarded as the average entanglement length:[21]

$$G_0 = \frac{k_B t}{\xi_H^{\ 3}}$$

where k_B stands for Boltzmann's constant. Taking for $G_0 = 117$ Pa, $T = 283$ K, and $k_B = 1.38 \times 10^{-23}$ SI, one finds $\xi_H = 32$ nm.

3.2.3. Stress Cycle. Starting from $\sigma_M = 10$ Pa, the sample is at first subjected to a decreasing shear stress σ down to different minima σ_m (step 1); σ is then kept constant for 60 min (step 2), and finally the stress is gradually brought back to the maximum σ_M (step 3). The temperature is kept constant at 20 °C, the concentration is 20 wt %, and the duration of a whole cycle is 4020 s.

Figure 5 displays the variations of the apparent viscosity versus the stress during the three step cycle experiment for two temperatures: 20 °C (Figure 5a) and 10 °C (Figure 5b).

During the first step, the apparent viscosity η is constant over the entire stress range: the solution is clearly Newtonian. During step 2, σ is kept constant and η increases sharply and reaches a value much larger than the constant apparent viscosity of step 1. Finally, during the last step, η decreases again and, in the high stress range, both viscosity curves $\eta(\sigma)$ superimpose again.

The highest stress value σ_M is always the same (10 Pa) as is the duration of step 2 (3600 s), but different values have been chosen for σ_m: 1, 0.1, and 0.01 Pa. Although the whole cycle is rather long, no significant increase of the apparent viscosity due to evaporation is seen in the high stress range after step 3 since the two distributions are well superimposed. We also noticed that the viscosity increase in step 2 depends, for a given temperature, on the value of σ_m, and as σ_m becomes larger, the increase of the viscosity becomes smaller. For a temperature of 10 °C and $\sigma_m = 1$ Pa, step 2 even disappears; it thus seems that a yield stress exists between 1 and 0.1 Pa. It should be emphasized that the highest values of η in step 2 do not have any physical meaning; they are the results of the computation of the ratio $\sigma/\dot{\gamma}$ with $\dot{\gamma}$ getting very small and unreliable as the viscosity increases. We thus formulate the hypothesis that the increase of the viscosity is due to the building up of aggregates, due to weak forces between the micelles.

3.3. Flow Birefringence Experiments. As quoted before, the flow birefringence experiments are performed on a simple polarimetric bench and the two quantities of interest, i.e., χ and Δn, are merely computed from the measurements done using the method of Senarmont.[22]

Parts a and b of Figure 6 respectively report the variations of the extinction angle χ and of the birefringence intensity Δn

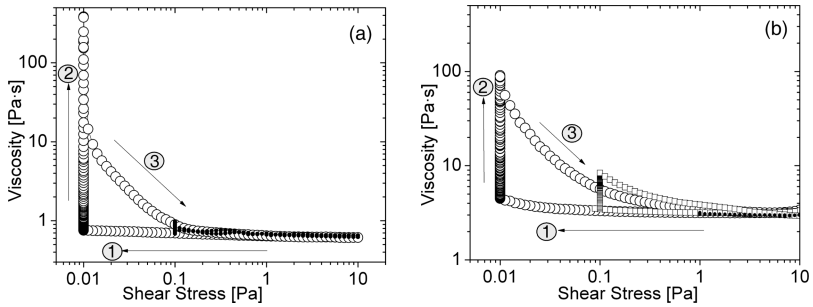

Figure 5. Apparent viscosity η as a function of the shear stress σ during the three step cycle for a sample at 20 wt %: step 1, decreasing stress from $\sigma_M = 10$ Pa to σ_m; step 2, constant stress at σ_m; step 3, increasing stress up to σ_M. (a) $T = 20$ °C, σ_m = (●) 0.1 and (○) 0.01 Pa; (b) $T = 10$ °C, σ_m = (○) 0.01, (□) 0.1, and (●) 1 Pa.

dx.doi.org/10.1021/jp2062139 | J. Phys. Chem. B 2012, 116, 1544–1550

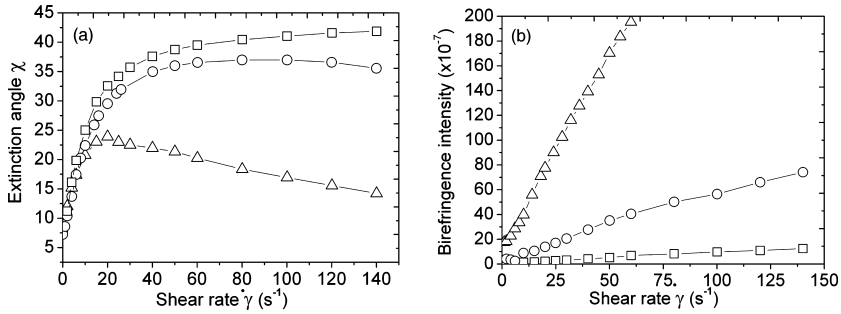

Figure 6. Flow birefringence experiments: (a) extinction angle χ; (b) birefringence intensity Δn versus the shear rate. The concentration is 20 wt % and the temperature is (△) 10, (○) 20, and (□) 30 °C.

versus the shear rate for three temperatures of 10, 20, and 30 °C.

Starting from a few degrees, χ increases at first in the low shear rate range with the same evolution for the three temperatures. Upon increasing the shear rate, the angle of the solution at 10 °C reaches a sharp maximum at $\dot{\gamma} \approx 20$ s^{-1}, before decreasing again in a quasi-linear way; for the two highest temperatures, the evolution is slightly different. At 20 °C, the maximum is broader, occurring approximately for $\dot{\gamma} \approx 80$ s^{-1}, and χ decreases slowly in the high shear rate domain. Finally, at 30 °C, no clear maximum is observed but the angle tends smoothly toward a plateau value close to 40°. This peculiar evolution of the extinction angle χ completely disagrees with the orientation theory of the streaming birefringence, which states that the angle should decrease from 45° toward 0 with the shear rate. A similar unexpected evolution of χ has already been reported in aluminum soap solutions subjected to shear flows[23] and in amylase in ethylenediamine-glycol.[24] In the orientation theory of birefringence, a value of the extinction angle close to 45° is an indication of small particles poorly orientated in the flow. The birefringence intensity Δn is increasing linearly in the whole shear rate range for the three temperatures, and for a given shear rate, Δn is all the smaller as the temperature is the higher. As a matter of fact, this is merely the result of the increasing influence of the Brownian motion at high temperature probably due to the existence of smaller micelles as suggested by the small value of Δn. At moderate shear rates ($\dot{\gamma} \approx 25$ s^{-1}) and 10 °C, the order of magnitude of Δn is $\approx 10^{-5}$; this value can be regarded as very high for liquids. Δn is also found to be negative; thus the main contribution comes from the intrinsic birefringence of the particles. In the near future, we propose to carry out further experiments, birefringence and light scattering, with solutions in the L_1 domain. We thus hope to bring a final conclusion and explanation of these unusual optical experimental results.

4. CONCLUSION

In this study, we investigated the steady state and dynamic rheological properties of binary solutions of the fluorinated surfactant $R_7^F(EO)_8$ in water. This surfactant is known to form self-assembled structures in water. First, we checked the phase diagram and determined the miscibility curve with a critical point at a temperature of 34 °C and $R_7^F(EO)_8$ concentration of 1 wt %. For a temperature below the cloud point and $R_7^F(EO)_8$ concentrations of <50 wt %, the L_1 isotropic phase is formed at rest. Several solutions in the L_1 domain have been prepared in order to study their rheological behavior. For steady shear measurements at a given temperature, the apparent viscosity increase with the concentration may be due to the increase of the micelle size or of the number of particles in the solution. At a given concentration (20 wt %), the apparent viscosity η increases with increasing temperature in the low shear rate range. Thus the solution at 40 °C shows a viscosity higher than those of the others; the same holds for the solution at 30 °C. Under oscillatory flow within the linear region, the loss modulus G'' always prevails over G' at 20 °C: the viscous-like character is dominant throughout the tested frequencies at this temperature. For the solution at 20 wt % in surfactant, G' remains well below G'' for the two highest temperatures. At 10 °C, however, a crossover is observed between G' and G'': the solution shows a Maxwellian character generally due to the presence of long entangled micelles. We also performed preliminary birefringence experiments to follow the variations of the extinction angle and of the birefringence intensity with the shear rate. The angle χ does not follow the predictions of the orientation theory: close to a few degrees in the low shear rate range, it increases at first with the shear rate. These original experiments bring a new point of view of the micellar structure: a small value of χ at low shear rates reveals the existence of large structures almost parallel to the flow direction and which could be disorganized by the increasing shear rate. This is quite inconsistent with wormlike micelles which are isotropic at rest and even under very low shear rate. Moreover, when subjected to a constant stress during the stress cycle experiments, the apparent viscosity η increases versus the time; turning down the hypothesis of evaporation, this shear thickening phenomenon could result from the emergence and growth of a structure. We think that this structure could be a weak micellar network.

■ ACKNOWLEDGMENTS

The authors thank DuPont de Nemours Belgium for providing the $R_7^F(EO)_8$ used in this study.

■ REFERENCES

(1) Kresge, C. T.; Leonowicz, M. E.; Roth, W. J.; Vartuli, J. C.; Beck, J. S. *Nature* **1992**, *359*, 710−712.
(2) Rousset, A. *Actual. Chim.* **2005**, *288*, 15−25.
(3) Blin, J. L.; Bleta, R.; Ghanbaja, J.; Stébé, M. J. *Microporous Mesoporous Mater.* **2006**, *94*, 74−80.
(4) Brinker, C. J., Scherer, G. W. *The Physics and Chemistry of Sol-Gel Processing*; Academic Press: San Diego, CA, 1990.
(5) Beck, J. S.; Vartuli, J. C.; Roth, W. J.; Leonowicz, M. E.; Kresge, C. T.; Schmitt, K. D.; Chu, C. T. W.; Olson, D. H.; Sheppard, E. W. *J. Am. Chem. Soc.* **1992**, *114*, 10834−10843.
(6) Huo, Q.; Margolese, D.; Ciesla, U.; Feng, J.; Gier, T. E.; Sieger, P.; Leon, R.; Petroff, P. M.; Schüth, F.; Stucky, G. D. *Nature* **1994**, *368*, 317−321.

(7) Tanev, P. T.; Chibwe, M.; Pinnavaia, T. J. *Nature* **1994**, *368*, 321−323.
(8) Kipkemboi, P.; Fogden, A.; Alfredsson, V.; Flodström, K. *Langmuir* **2001**, *17*, 5398.
(9) Zhao, D.; Huo, Q.; Feng, J.; Chmelka, B. F.; Stucky, G. D. *J. Am. Chem. Soc.* **1998**, *120*, 6024.
(10) Blin, J. L.; Bleta, R.; Stébé, M. J. *J. Colloid Interface Sci.* **2006**, *300*, 765.
(11) Michaux, F.; Blin, J. L.; Stébé, M. J. *Langmuir* **2007**, *23*, 831.
(12) Michaux, F.; Blin, J. L.; Stébé, M. J. *J. Phys. Chem. B* **2008**, *112*, 11950.
(13) Mitchell, D. J.; Tiddy, G. J. T.; Waring, L.; Bostock, T.; McDonald, M. P. *J. Chem. Soc., Faraday Trans. 1* **1983**, *79*, 975−1000.
(14) Zhao, D.; Huo, Q.; Feng, J.; Chmelka, B. F.; Stucky, G. D. *J. Am. Chem. Soc.* **1998**, *120*, 6024−6036.
(15) Kim, J. M.; Sakamoto, Y.; Hwang, Y. K.; Kwon, Y. U.; Terasaki, O.; Park, S. E. *J. Phys. Chem. B* **2002**, *106*, 2552−2558.
(16) Maclay, W. N. *J. Colloid Sci.* **1956**, *11*, 272−285.
(17) Bleta, R.; Blin, J. L.; Stébé, M. J. *J. Phys. Chem. B* **2006**, *110*, 23547−23556.
(18) Shinoda, K. *Principles of Solution and Solubility*; Lagowski, J. J., Ed.; Marcel Dekker: New York, 1978.
(19) Shrestha, R. G.; Shrestha, L. K.; Sharma, S. C.; Aramaki, K. *J. Phys. Chem. B* **2008**, *112*, 10520−10527.
(20) Cates, M. E.; Candau, S. J. *J. Phys.: Condens. Matter* **1990**, *2*, 6869−6892.
(21) Doi, M.; Edwards, S. F. *The Theory of Polymer Dynamics*: Clarendon Press: Oxford, 1986.
(22) Senarmont, D. E. *Ann. Chem. Phys.* **1840**, *73*, 337.
(23) Gray, V. R.; Alexander, A. E. *J. Phys. Chem.* **1949**, *53* (1), 9−22.
(24) Foster, J. F.; Zucker, D. *J. Phys. Chem.* **1952**, *56* (2), 174−177.